Prepared for submission to JCAP

arXiv:2412.01219v2 [astro-ph.CO] 16 Aug 2025

Estimating the gravitational wave background anisotropy: a Bayesian approach boosted by cross-correlation angular power spectrum

Chi Tian,[a] **Ran Ding,**[a,1] **and Xiao-Xiao Kou**[b,1]

[a]School of Physics and Optoelectronics Engineering, Anhui University, 111 Jiulong Road, Hefei, Anhui, 230601, China

[b]School of Physics and Astronomy, University of Minnesota, Minneapolis, MN 55455, USA

E-mail: ctian@ahu.edu.cn, dingran@mail.nankai.edu.cn, kou00016@umn.edu

Abstract. We introduce a new method designed for Bayesian inference of the angular power spectrum of the Gravitational Wave Background (GWB) anisotropy. This scheme works with detector data and can optionally incorporate the cross-correlations between the GWB anisotropy and other cosmological tracers, enhancing the significance of Bayesian inference. We employ the realistic LISA response and noise model to demonstrate the validity of this approach. The findings indicate that, for the injected cosmological GWB signal, without considering any cross-correlations, the 4-year LISA data is insufficient to achieve a significant detection of multipoles. However, if the anisotropies in the GWB are strongly correlated with the Cosmic Microwave Background (CMB), the 4-year data can provide unbiased estimates of the quadrupole moment ($\ell = 2$). This reconstruction process is generic and not restricted to any specific detector, offering a new framework for extracting anisotropies in the GWB data from various current and future gravitational wave observatories.

[1]Corresponding authors.

Contents

1 Introduction 1

2 Anisotropic GWB intensity and detector data 2

3 Likelihood with cross-correlations 3

4 Bayesian inference of LISA mock data 6

5 Discussions 8

A From the anisotropic GW fractional energy density to the GW intensity 10

B Conditional probability distribution considering cross-correlations 13

C Likelihood function after marginalization 14

1 Introduction

Our ability to detect gravitational waves (GWs) will undoubtedly reach an unprecedented level in the next decade, with detection ranges spanning from nanohertz to several hundred hertz and significantly enhanced precision. This substantial advancement is likely to help us fully decipher a new background signal in the Universe — the gravitational wave background (GWB), whose preliminary clues have been revealed by recent Pulsar Timing Array (PTA) experiments [1–5]. This diffused GW signal, resulting from superpositions of numerous unresolved sources, can be classified into two categories: the astrophysical gravitational wave background (AGWB) and the cosmological gravitational wave background (CGWB). The former results from superpositions of unresolved galactic and extra-galactic sources, mostly related to the dynamics of compact objects [6–11]. The latter, originating from early Universe processes, is closely related to new physics, such as inflation, reheating/preheating, primordial black holes, topological defects, or cosmological first-order phase transitions [12–16].

Similar to the CMB and other cosmological probes, the GWB also carries anisotropies, which can originate from either source distributions or propagation processes. Anisotropies arising from sources include those generated by inhomogeneous distributions of compact objects [17], in the case of the AGWB, or those resulting from large scale perturbations introduced by domain walls in the early universe [18], as in the CGWB. On the other hand, the propagation process may lead to anisotropies due to various gravitational effects, analogous to the CMB photons [19]. Considerable efforts have been made in recent years to model the angular power spectrum of the GWB anisotropy [20–41] and to assess its detectability in the operating and proposed GW observations through estimating the signal-to-noise ratio (SNR) [42–48]. Meanwhile, to quantitatively extract anisotropic information from the data, both Bayesian and frequentist frameworks for constructing GWB sky maps have been developed [49–57]. However, existing Bayesian map-making techniques, which rely on constructing the entire sky map using the spherical harmonic approach, often encounter challenges such as slow convergence (see discussions in [57]). Given that many physical models predict the power spectrum, a Bayesian framework designed to extract the angular

spectrum directly from detector data could be more suitable and convenient for exploring these models. Moreover, as predicted by many theoretical studies [25, 44, 58–60], regardless of their astrophysical or cosmological origins, the anisotropies in the GWB generally exhibit significant cross-correlations with other existing cosmological tracers, such as the CMB, the CMB lensing, or large-scale structures. The detection sensitivity to the anisotropies would undoubtedly benefit from these potential cross-correlations, as suggested by [42, 44, 45], through estimating the enhanced SNR. Nevertheless, a consistent methodology for integrating these cross-correlations into the data analysis framework, facilitating the extraction of the angular power spectrum of the GWB anisotropy, has not been established.

In this study, we focus on a novel data analysis scheme designed to extract anisotropies in the form of the angular power spectrum from data of GW detectors without constructing any sky map. This framework optionally accounts for the potential cross-correlations between the GWB anisotropy and other cosmological tracers. We demonstrate the validity of this approach by applying it to LISA [61–63] mock data and discuss its broader applications for future GW observations.

2 Anisotropic GWB intensity and detector data

Assuming the GWs to be Gaussian, stationary and unpolarized, the metric perturbation $h_p(f, \hat{\mathbf{n}})$ in Fourier space can be characterized by its quadratic expectation values as

$$\left\langle h_p(f, \hat{\mathbf{n}}) h^*_{p'}\left(f', \hat{\mathbf{n}}'\right)\right\rangle \equiv \delta(f - f') \frac{\delta^2\left(\hat{\mathbf{n}}, \hat{\mathbf{n}}'\right)}{4\pi} \mathrm{W}_{pp'}(f, \hat{\mathbf{n}}), \tag{2.1}$$

where $p = \{+, \times\}$ labels the polarization states, $\hat{\mathbf{n}}$ is the direction of propagation in the sky and the matrix W is related to the gravitational Stokes parameters Q, U, and V. Under the unpolarized condition, $Q = U = V = 0$, one has $\mathrm{W}_{++,\times\times}(f, \hat{\mathbf{n}}) = I(f, \hat{\mathbf{n}})$, where $I(f, \hat{\mathbf{n}})$ represents the GW intensity.

On the other hand, when considering the GWB, it's a common practice to quantifying it through the fractional energy density Ω_{rmGW}, whose spectrum can be separated into a background part (monopole) and a linear fluctuation. It can be proven [52, 64] the relationship between the anisotropic GW intensity and the fractional energy density, using the spherical harmonic coefficients, can be expressed by (see Appendix A for the detailed derivation)

$$I_{00}(f) \equiv \frac{3H_0^2}{4\pi^2} \frac{\overline{\Omega}_{\mathrm{GW}}(f)}{f^3}, \tag{2.2}$$

and

$$\begin{aligned} I_{\ell m}(f) &= \frac{3H_0^2}{4\pi^2} \frac{\overline{\Omega}_{\mathrm{GW}}(f)}{\sqrt{4\pi} f^3} \left(4 - \frac{\partial \ln \overline{\Omega}_{\mathrm{GW}}(f)}{\partial \ln f}\right) a^{\mathrm{GW}}_{\ell m} \\ &\equiv K_f a^{\mathrm{GW}}_{\ell m}, \end{aligned} \tag{2.3}$$

where we have assumed that K_f has encapsulated all the frequency dependencies, leaving $a^{\mathrm{GW}}_{\ell m}$s frequency-independent [65, 66]. Our aim is to extract the power spectrum of $a^{\mathrm{GW}}_{\ell m}$, denoted as C^{GW}_{ℓ}, from the GWB data.

Our data analysis is based on the short-time Fourier transform (STFT) data of a GW detector A, denoted as $d^A_i(f)$, which is obtained by applying Fourier transforms to the time-

series signal over a specific time segment $T_{\rm seg}$, around a given time frame t as

$$d_t^A(f) = \int_{t-T_{\rm seg}/2}^{t+T_{\rm seg}/2} dt' e^{-2i\pi f t'} d^A(t'). \tag{2.4}$$

Note that $T_{\rm seg}$ also determines the width of frequency bins $\Delta f = 1/T_{\rm seg}$ and $d_t^A(f)$ can be estimated through

$$d_t^A(f) = \int d^2\Omega_{\hat{\mathbf{n}}} \sum_p R_{t,p}^A(f,\hat{\mathbf{n}}) h_p(f,\hat{\mathbf{n}}) + n_{t,f}^A \,, \tag{2.5}$$

where $R_{t,p}^A(f,\hat{\mathbf{n}})$ and $n_{t,f}^A$ are the response function and noise for the detector A. $d_t^A(f)$ has a zero mean, and its ensemble average, evaluated at equal time frame t (and is otherwise zero), can be estimated by

$$\begin{aligned}\left\langle d_t^A(f) d_t^{B*}\left(f'\right)\right\rangle &= \delta(f-f')\left[\sum_{\ell=0}^{\infty}\sum_{m=-\ell}^{\ell}\gamma_{\ell m}^{AB}(t,f) I_{\ell m}(f) + N_{t,f}^{AB}\right] \\ &\equiv \frac{\delta_{ff'}^K}{\Delta f}\langle D_{t,f}^{AB}\rangle \,,\end{aligned} \tag{2.6}$$

where the Dirac delta function $\delta(f-f')$ is replaced by Kronecker delta δ^K through $\delta(f-f') = \delta_{ff'}^K/\Delta f$, and $\langle n_{t,f}^A n_{t,f'}^{B*}\rangle \equiv \delta(f-f') N_{t,f}^{AB}$ represents the noise power spectral density (PSD) for the detector pair AB, and $\gamma_{\ell m}^{AB}(t,f)$ are spherical harmonic coefficients of the response function $\gamma_{t,f}^{AB}(\hat{\mathbf{n}})$ for this detector pair, defined by

$$\gamma_{t,f}^{AB}(\hat{\mathbf{n}}) = \Delta\Omega \sum_p R_{t,p}^A(f,\hat{\mathbf{n}}) R_{t,p}^{B*}(f,\hat{\mathbf{n}}) \,. \tag{2.7}$$

In similar manner, the covariance of $D_{t,f}^{AB}$ can be written as

$$C_{t,f}^{ABCD} \equiv \langle D_{t,f}^{AB}, D_{t,f}^{CD*}\rangle \approx \left(\gamma_{00}^{AC}(t,f) I_{00}(f) + N_{t,f}^{AC}\right)\left(\gamma_{00}^{DB}(t,f) I_{00}(f) + N_{t,f}^{DB}\right) \,, \tag{2.8}$$

where the approximation adopted is based on the fact that the contribution from multipoles are subdominant compared to the those from monopole. As a consequence, the information of anisotropies is exclusively encoded in $\langle D_{t,f}^{AB}\rangle$. Note that while a diagonalized covariance matrix is often employed, such as the time-delay interferometry (TDI) channels frequently used in the LISA literature, this formalism is more general. It does not require a diagonalized covariance matrix and inherently accounts for cross-detector correlations. The conversion between our scheme and the TDI channels can be found in [43].

3 Likelihood with cross-correlations

Our aim is to perform Bayesian estimations on the angular power spectrum of the GWB anisotropy using the detector dataset $D_{\{t,f\}}^{\{AB\}}$. For this purpose, a practical likelihood function is necessary. When a set of $I_{\{\ell m\},f}$ is given, the likelihood for $D_{t,f}^{\{AB\}}$, which represents data for various detector's combinations at a specific time and frequency, can be simply written as

$$\begin{aligned}&\mathcal{L}\left(D_{t,f} \mid I_{\{\ell m\},f}\right). \\ &= \prod_{AB,CD} \frac{1}{\left|\pi C_{t,f}^{ABCD}\right|} \exp\left\{-\left(D_{t,f}^{AB} - \langle D_{t,f}^{AB}\rangle\right)^\dagger \left(C_{t,f}^{ABCD}\right)^{-1}\left(D_{t,f}^{CD} - \langle D_{t,f}^{CD}\rangle\right)\right\}.\end{aligned} \tag{3.1}$$

Note that this likelihood is valid only when $D^{\{AB\}}_{\{t,f\}}$ are Gaussian, which is approximately the case when considering $D^{\{AB\}}_{\{t,f\}}$ as the average of multiple samples. However, for a given angular power spectrum $C^{\rm GW}_{\{\ell\}}$, there are in principle an infinite number of realizations in terms of $I_{\{\ell m\}}$, making it challenging to write down a likelihood function that directly links the detector data with a model predicted $C^{\rm GW}_{\{\ell\}}$. Therefore, we must remain agnostic regarding specific realizations.

In addition, the GWB anisotropy can be correlated with another known cosmological tracer Y. When neglecting potential non-Gaussianities, analogous to studies investigating the cross-correlation between the CMB and other probes (i.e. [67–69]), we assume that the maps of the GWB and the tracer Y can be described by multivariate Gaussian variables. Their covariance is determined by their auto angular spectra $C^{\rm GW}_\ell$, $C^{\rm Y}_\ell$ and the cross spectrum $C^{\rm GW\times Y}_\ell$. Consequently, the conditional probability for the GWB can be derived with the knowledge of Y, whose measured spherical harmonics coefficients are $a^{\rm Y}_{\{lm\}}$ with negligible uncertainties compared to the GWB measurements. It can be proven (see Appendix B for the detailed derivation) that for a given condition characterized by the combination of $\left(a^{\rm Y}_{\{\ell m\}}, C^{\rm GW}_{\{\ell\}}, C^{\rm GW\times Y}_{\{\ell\}}\right)$, the conditional distribution of $I_{\{\ell m\}}$ at a given frequency, denoted as $\mathcal{L}\left(I_{\{\ell m\},f} \mid {\rm GW}\times{\rm Y}\right)$, obeys

$$\mathcal{L}\left(I_{\{\ell m\},f} \mid {\rm GW}\times{\rm Y}\right) = \prod_{\substack{\ell m\\ \ell\geq 1}} \frac{1}{\pi C^{\rm GW|Y}_\ell} \exp\left(-\frac{\left|I_{\ell m,f} - K_f \mu^{\rm GW|Y}_{\ell m}\right|^2}{K_f^2 C^{\rm GW|Y}_\ell}\right), \tag{3.2}$$

where we have defined the mean and the auto-correlation of this GWB anisotropy as

$$\mu^{\rm GW|Y}_{\ell m} \equiv \frac{C^{\rm GW\times Y}_\ell}{C^{\rm Y}_\ell} a^{\rm Y}_{\ell m}\,, \tag{3.3}$$

$$\begin{aligned} C^{\rm GW|Y}_\ell &\equiv C^{\rm GW}_\ell - \frac{\left(C^{\rm GW\times Y}_\ell\right)^2}{C^{\rm Y}_\ell} \\ &= C^{\rm GW}_\ell \left[1 - \left(r^{\rm GW\times Y}\right)^2\right], \end{aligned} \tag{3.4}$$

for $\ell \geq 1$, and the relative cross-correlation $r^{\rm GW\times Y}$ is defined by $r^{\rm GW\times Y} \equiv C^{\rm GW\times Y}_\ell / \sqrt{C^{\rm GW}_\ell C^{\rm Y}_\ell}$. Note that since the intensity monopole I_{00} is related to the GW fractional energy, as in eq. (2.2), the product in eq. (3.2) does not include the $\ell = 0$ term. For the sake of conciseness and computational convenience, we introduce the following compact notations. We use Latin letters, such as a and b, to compress the detector combinations, such as AB, into a single index. Additionally, we use Greek letters μ, ν, etc., to denote combinations of ℓm s. To be

specific, we have:

$$
\begin{aligned}
a = \{AB\} &= \underbrace{\{1,1\},\{1,2\},\cdots,\{1,n\},\cdots,\overbrace{\{n,1\},\cdots,\{n,n\}}^{n\,\text{terms}}}_{n\times n\,\text{terms}}, \\
\mu = \{\ell m\} &= \underbrace{\{1,-1\},\{1,0\},\{1,1\},\cdots,\overbrace{\{\ell_{\max},-\ell_{\max}\},\cdots,\{\ell_{\max},\ell_{\max}\}}^{(2\ell_{\max}+1)\,\text{terms}}}_{\ell_{\max}(\ell_{\max}+2)\,\text{terms}}, \\
&\Gamma_{a0} \equiv \gamma_{00}^{\{AB\}}, \quad \Gamma_{a\mu} \equiv \gamma_{\{\ell m\}}^{\{AB\}}, \quad X_0 = \overline{X}_0 \equiv I_{00}, \quad X_\mu \equiv I_{\{\ell m\}}, \quad \overline{X}_\mu \equiv K_f \mu_{\{\ell m\}}^{\mathrm{GW|Y}}, \\
&D_a \equiv D_{tf}^{AB}, \quad N_a \equiv N_f^{AB}, \quad S_a \equiv \langle D_{tf}^{AB} \rangle = \Gamma_{a0} X_0 + \Gamma_{a\mu} X_\mu + N_a, \quad (C_D)_{ab} \equiv C_{t,f}^{ABCD}, \\
&(C_I)_{\mu\nu} \equiv K_f^2 \mathrm{diag}\Big(\underbrace{C_1^{\mathrm{GW|Y}}, C_1^{\mathrm{GW|Y}}, C_1^{\mathrm{GW|Y}}, \cdots, \overbrace{C_{\ell_{\max}}^{\mathrm{GW|Y}}, \cdots, C_{\ell_{\max}}^{\mathrm{GW|Y}}}^{(2\ell_{\max}+1)\,\text{terms}}}_{\ell_{\max}(\ell_{\max}+2)\,\text{terms}} \Big),
\end{aligned}
\tag{3.5}
$$

Following this convention, the likelihood functions in eqs. (3.1) and (3.2) are reformulated as

$$
\mathcal{L}\left(D_{t,f} \mid I_{\{\ell m\},f}\right) = \frac{1}{|\pi C_D|} \exp\Big\{ -\Big(D_a - S_a\Big)^\dagger (C_D)^{-1}_{ab} \Big(D_b - S_b\Big) \Big\}, \tag{3.6}
$$

$$
\mathcal{L}\left(I_{\{\ell m\},f} \mid \mathrm{GW}\times\mathrm{Y}\right) = \frac{1}{|\pi C_I|} \exp\Big\{ -\Big(X_\mu - \overline{X}_\mu\Big)^\dagger (C_I)^{-1}_{\mu\nu} \Big(X_\nu - \overline{X}_\nu\Big) \Big\}\,. \tag{3.7}
$$

To finally derive the likelihood for the entire data set $D_{\{t,f\}}$ while remaining agnostic to the specific realization, we marginalize over all $I_{\ell m}$s and sum over contributions from all time frames and frequency bins by computing

$$
\begin{aligned}
\mathcal{L}\Big(D_{\{t,f\}}\Big|\mathrm{GW}\times\mathrm{Y}\Big) &\propto \prod_{t,f} \int \mathcal{D} I_{\substack{\ell m,f \\ \ell\geq 1}} \mathcal{L}\left(D_{t,f}\Big|I_{\{\ell m\},f}\right) \mathcal{L}\left(I_{\{\ell m\},f} \mid \mathrm{GW}\times\mathrm{Y}\right) \\
&= \prod_{t,f} \frac{1}{|\pi C_D||\pi C_I|} \int \Big[\prod_{\ell=1}^{\ell_{\max}} \prod_{m=-\ell}^{\ell} d^2 X_\rho \Big] \exp\Big\{ -\Big(D_a - \overline{X}_0 \Gamma_{0a} - X_\mu \Gamma_{\mu a} - N_a\Big)^* (C_D)^{-1}_{ab} \\
&\quad \Big(D_b - \Gamma_{b0}\overline{X}_0 - \Gamma_{b\nu} X_\nu - N_b\Big) - \Big(X_\mu - \overline{X}_\mu\Big)^\dagger (C_I)^{-1}_{\mu\nu} \Big(X_\nu - \overline{X}_\nu\Big) \Big\},
\end{aligned}
\tag{3.8}
$$

where $d^2 X_\rho = d\mathrm{Re}X_\rho d\mathrm{Im}X_\rho$, and the dimension of the integral is $d = \ell_{\max}(\ell_{\max}+2)$. By plugging in the expression from eqs. (2.6), (2.8), (3.6) and (3.7), and after some algebra, we finally arrive at a very compact form of the likelihood function (see Appendix C for detail derivations):

$$
\mathcal{L}\left(D_{\{t,f\}} \mid \mathrm{GW}\times\mathrm{Y}\right) \propto \prod_{t,f} |\pi C_{ab}|^{-1} \exp\Big(-J_a^\dagger C^{-1}_{ab} J_b\Big)\,, \tag{3.9}
$$

$$
C_{ab} = (C_D)_{ab} + \Gamma_{a\mu} (C_I)_{\mu\nu} \Gamma^*_{\nu b}\,, \tag{3.10}
$$

$$
J_a = D_a - \Gamma_{a\mu} \overline{Z}_\mu - N_a\,. \tag{3.11}
$$

Note that all quantities in eq. (3.9) depend on the time and frequencies. we have also defined $\overline{Z}_\mu \equiv \mu_{\ell m}^{\mathrm{GW|Y}}$ for $\ell, \mu \geq 1$ and $\overline{Z}_0 \equiv I_{00}$ (see eq. (2.2)) for $\ell, \mu = 0$.

Eqs. (3.9) to (3.11) consist the main results of this study. It is also important to know that this likelihood is generic, being applicable to models that are not considering any cross-correlations. In such case, one has $C_\ell^{\rm GW\times Y}=0$, and the mean and the covariance of harmonic coefficients are reduced to $\overline{Z}_\mu = K_f \mu_{\ell m}^{\rm GW|Y} = 0$ for $\mu \geq 1$ and $C_\ell^{\rm GW|Y} = C_\ell^{\rm GW}$, producing a likelihood function based on the GW angular power spectrum without considering any cross-correlations, similarly as the results in [55, 70].

4 Bayesian inference of LISA mock data

For demonstration purposes, we inject anisotropic GWB signals to LISA and attempt to estimate the injected anisotropic level. The injected signal has a power-law spectrum $\overline{\Omega}_{\rm GW}(f) = A(f/f_{\rm ref})^\alpha$, where we have chosen $A=10^{-10}$, $f_{\rm ref}=10^{-3}$ Hz and $\alpha=1$, as depicted in the upper panel of Fig. 1. The LISA power-law (PL) sensitivity curve (SNR=3 with 4-year observations), representing the detector's ability to measure a GWB spectrum in power-law form, is also presented in the same figure. It is a relatively strong signal compared to the LISA PL sensitivity and the predicted spectrum of compact binaries [6–10]. Therefore, this mock signal can be considered as a GWB from new physics, which may arise from first order phase transitions or inflationary models (see [71, 72] for comprehensive reviews) .

The anisotropies in the signal are generated based on a scale invariant angular spectrum of $a_{\ell m}^{\rm GW}$s, implying that $\widetilde{C}_\ell^{\rm GW} \equiv \ell(\ell+1)C_\ell^{\rm GW} = {\rm Const.}$ This is a typical approximated prediction of many cosmological models at low ℓs [25, 44, 59], capturing propagation effects such as Sachs-Wolfe or Integrated Sachs-Wolfe contributions, along with anisotropies originating from sources. Our primary task is to estimate the $\widetilde{C}_\ell^{\rm GW}$ from the mock data. To this end, we generate a data set $\{d_A^t(f)\}$ following the covariance given by eq. (2.6) in the frequency range $f\sim[0.0001, 0.2]\,{\rm Hz}$ with $\Delta f = 10^{-6}\,{\rm Hz}$. This frequency spacing corresponds to an observation segment $T_{\rm seg}\sim 11\,{\rm days}$, generating 25 different observation segments in a year, corresponding to a 75% observation efficiency. Each segment has a different antenna pattern due to the satellite array's varying orientations over a year. We compute the LISA response and the noise PSD using the public code `schNell` [43], which estimates the LISA time-dependent response function based on spacecraft positions over time, as derived in [74], while assuming time-independent noise [64]. Once the fiducial data is injected, we first attempt to recover the monopole spectrum of the signal (see Fig. 1). This can be simply done by employing eq. (3.9) and setting $C_{\mu\nu}^I$ to zero. The nearly invisible shaded region indicates that the uncertainties in the reconstructed monopole signals are negligible. The small uncertainties suggest that the contributions from the multipoles in the likelihood can be safely ignored when inferring the monopole spectrum. We therefore fix the reconstructed monopole parameters during the subsequent inferences of the angular power spectrum.

We then employ the full likelihood in eq. (3.9) to estimate the magnitude of the lowest several multipoles. To avoid potential numerical instabilities in the matrix inverses, in our calculation, we inverse matrices by expanding the term $\Gamma_{a\mu}C_{\mu\nu}^I\Gamma_{\nu b}^*$ in eq. (3.10) to the 2nd order. The resulting posteriors are presented in Fig. 2. It is apparent that, with the injected anisotropic level in the cosmological GWB, the LISA 4-year mission lacks sufficient sensitivity to recover the magnitude of multipoles. This finding is consistent with previous studies [42, 45, 48] that are based on the SNR analysis. Note that we only present the results for even multipoles, as the even parity of the LISA antenna patten results in a weak SNR in the odd multipoles. We also find that unrealistically extending the LISA mission to 80 years and increasing the anisotropic level to $\log_{10}\widetilde{C}_\ell^{\rm GW}=-1.6$ will result in a restrictive posterior

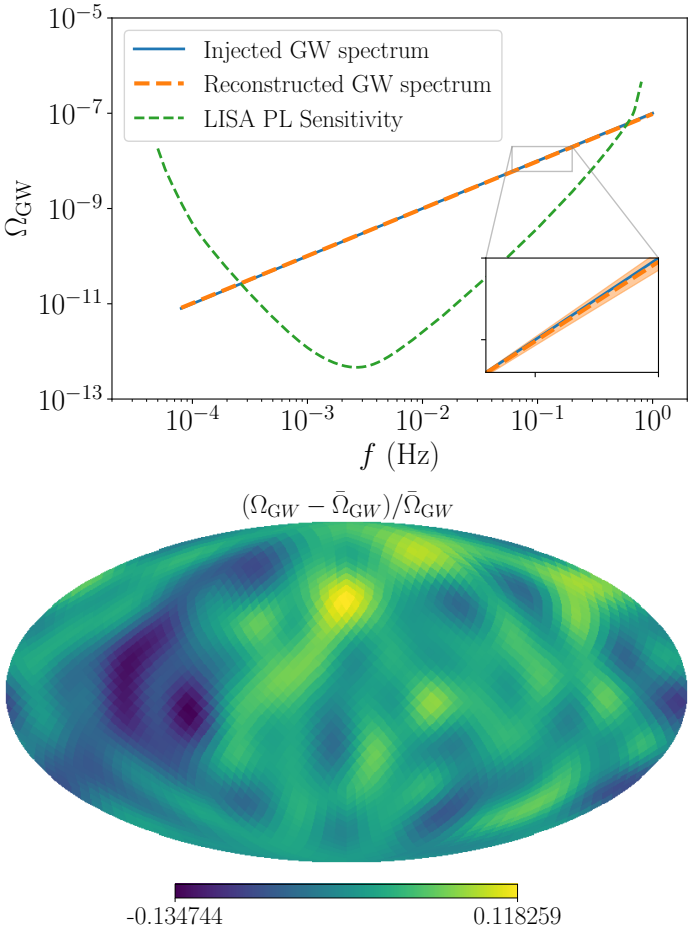

Figure 1. Upper Panel: Injected and reconstructed GWB spectrum. The 1σ uncertainty of the reconstruction is represented by the nearly invisible shaded region; Lower Panel: The sky map of the fluctuation of injected GWB ($(\Omega_{GW} - \bar{\Omega}_{GW})/\bar{\Omega}_{GW}$), whose $\log_{10} \widetilde{C}_\ell^{\rm GW} = -2.4$. Locations of map pixels are following the `HealPix`[73] convention with $N_{\rm side} = 16$.

for the quadrupole moment $\widetilde{C}_2^{\rm GW}$, whose 1σ region is comparable to the cosmic variance $\sigma_{\widetilde{C}_\ell^{\rm GW}} = \sqrt{2/(2\ell+1)}\widetilde{C}_\ell^{\rm GW}$ [75], thereby confirming the validity of our scheme.

Depending on the sources, the anisotropies in the GWB generally show different levels of cross-correlations with diverse cosmological tracers. For the CGWB, current models suggest that it has a strong correlation with the CMB or the CMB lensing [25, 44, 59]. To explore the most optimistic constraints on the LISA detectability based on known cross-correlations, we consider an ideal scenario in which the GWB is perfectly correlated with the CMB. Under this assumption, we inject a GWB fully correlated with the CMB by setting $r^{\rm GW\times CMB} = 1$, subsequently employing this scheme to infer the magnitude of the lowest several multipoles in the GWB. Our findings indicate that the LISA 4-year data is able to provide unbiased estimations of quadrupole $\widetilde{C}_2^{\rm GW}$ when $\log_{10} \widetilde{C}_\ell^{\rm GW} = -2.4$, as suggested by the upper panel in Fig. 3. As the bottom panel in Fig. 3 implies, this reconstruction works until $\widetilde{C}_\ell^{\rm GW}$ decreases to approximately $\log_{10} \widetilde{C}_\ell^{\rm GW} \simeq -4$.

We have also simulated a GWB map based on a smaller relative correlation with the CMB, specifically $r^{\rm GW\times CMB} = 0.85$ with $\log_{10} \widetilde{C}_\ell^{\rm GW} = -2.4$. By employing the likelihood

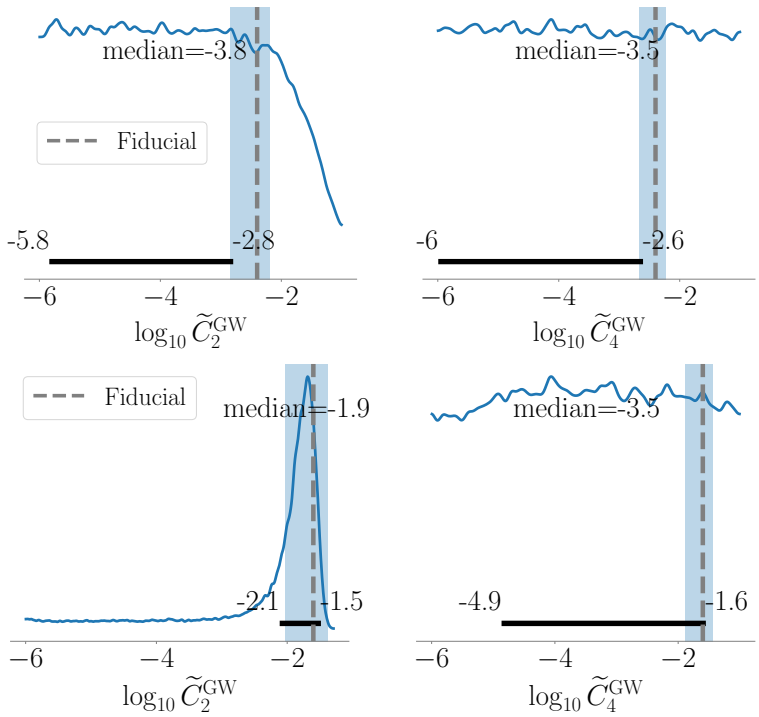

Figure 2. Upper Panel: Reconstructed multipoles $\widetilde{C}_2^{\rm GW}$ and $\widetilde{C}_4^{\rm GW}$ based on the LISA 4-year data. Fiducial $\log_{10}\widetilde{C}_\ell^{\rm GW} = -2.4$. Lower Panel: Reconstructed multipoles based on the LISA 80-year data. Fiducial $\log_{10}\widetilde{C}_\ell^{\rm GW} = -1.6$. The black bars on the bottom mark the 1σ region, and the shaded regions represent the cosmic variance.

function given in eq. (3.9) and taking $r^{\rm GW\times CMB}$ as a new parameter, we plot $r^{\rm GW\times CMB}$ vs. $\widetilde{C}_2^{\rm GW}$ contour in the left panel of Fig. 4. The results indicate that, even under the condition of a weaker correlation, our scheme remains effective in inferring quadrupole $\widetilde{C}_2^{\rm GW}$: the fiducial value can still be recovered within a 1σ confident level.

Lastly, we exam the scenario where the relative correlation is minimal ($r^{\rm GW\times CMB} = 0.0$). As indicated in the right panel of Fig. 4, due to the strong degeneracy between the strength of anisotropy and the correlation level (the smaller the anisotropy, the weaker the constraints on the cross-correlation), an upper limit for the relative correlation cannot be established. In addition, the overall constraints on the anisotropic level are similar to the case without considering the cross-correlation (see upper panel in Fig. 2).

5 Discussions

In this study, we introduce a novel scheme for performing Bayesian inference on the detector data associated with the stochastic gravitational wave background. Utilizing a new analytical likelihood function, this approach directly connects the GW data to the angular power spectrum, with the capability to incorporate the cross-correlations between the GWB anisotropy and any cosmological tracers. As a crucial feature of the GWB anisotropy, these cross-correlations, predicted by various physical models, can significantly enhance the reconstruction capability of our framework.

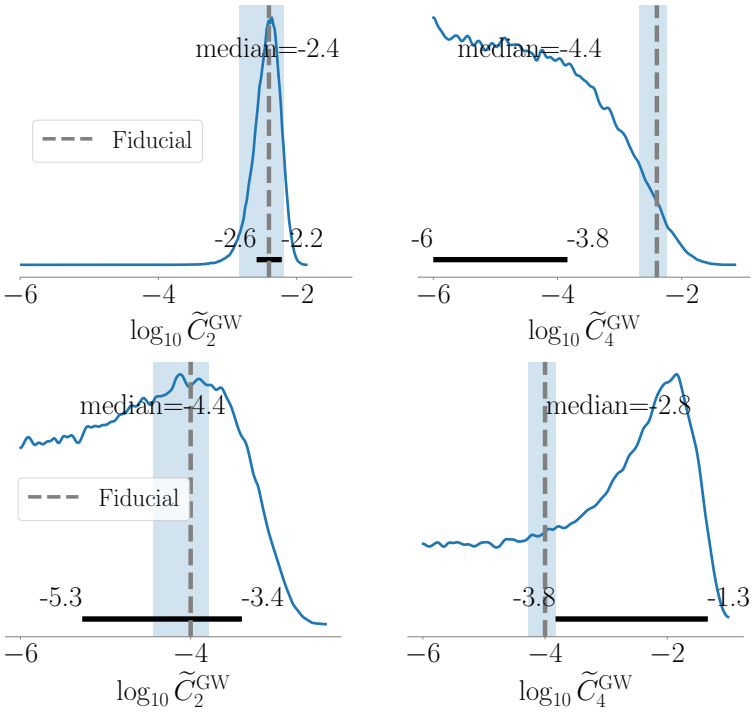

Figure 3. Reconstructed multipoles based on the LISA 4-year data, assuming a perfect cross-correlations between the GWB and the CMB. Upper Panel: The fiducial $\log_{10}\widetilde{C}_\ell^{\rm GW} = -2.4$. Lower Panel: The fiducial $\log_{10}\widetilde{C}_\ell^{\rm GW} = -4$. The black bars on the bottom mark the 1σ region, and the shaded regions represent the cosmic variance.

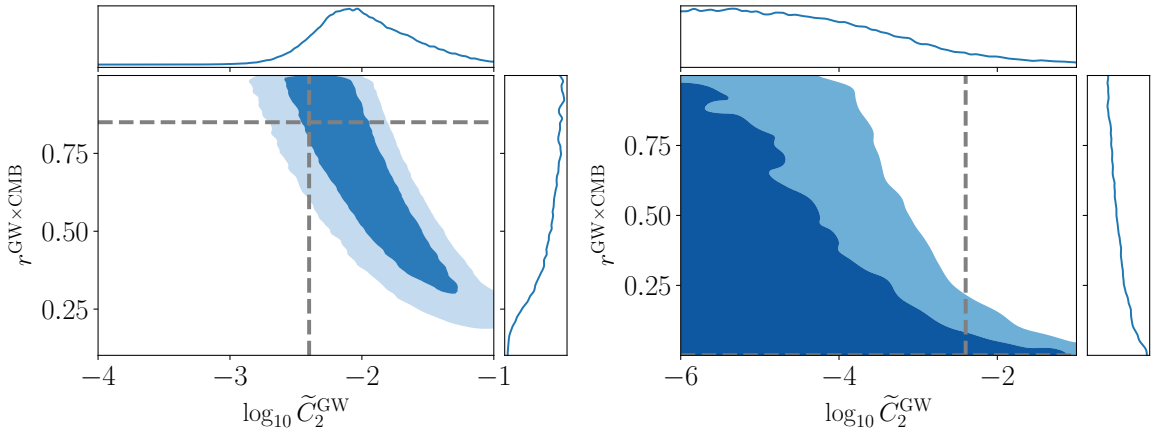

Figure 4. Contour and posterior plots of the quadrupole $\widetilde{C}_2^{\rm GW}$ and relative cross-correlation. Shaded regions represent the 1σ and 2σ range. Left Panel: Strong correlation case: the fiducial $r^{\rm GW\times CMB} = 0.85$ and $\log_{10}\widetilde{C}_\ell^{\rm GW} = -2.4$, denoted by the grey dashed lines. Right Panel: No correlation case: the fiducial $r^{\rm GW\times CMB} = 0$ and $\log_{10}\widetilde{C}_\ell^{\rm GW} = -2.4$, denoted by the grey dashed lines.

We employ forecasted LISA response and noise to demonstrate the validity of this approach. Our findings indicate that, for the injected cosmological GWB signal, without considering any cross-correlations, the noise level in the 4-year LISA data prevents us from constructing reliable Bayesian inference on multipoles unless the LISA mission is unrealistically extended to 80 years. However, if the anisotropies in the GWB are strongly correlated with another cosmological tracer, such as the CMB, the 4-year LISA data can provide unbiased estimates of the quadrupole moment. We emphasize that this study tests the validity of our scheme using mock data that excludes any foreground signals, which could potentially compromise the reconstruction accuracy or introduce bias into the results. Consequently, it is essential to apply appropriate foreground cleaning techniques prior to utilizing our scheme.

Bypassing the time-consuming map-making process, the posterior sampling based on this new framework is straightforward to implement, and typically completes within several hours. We also emphasize that this scheme is designed generically for arrays of GW detectors. Our work, therefore, paves the way for detailed studies of the detectability of anisotropies in current and future GW observations, such as LVK [76], TianQin [77], Taiji [78, 79], DECIGO [80], BBO [81], ET [82], and their possible joint searches [83–85], as well as PTA experiments. The exploration of open questions, such as how various GWB source models are constrained from the GWB anisotropy, or how to differentiate between astrophysical and cosmological sources based on the anisotropies, might benefit from this new scheme. However, the focus of this study is on the success of the method rather than the detectability for a specific detector or constraining GWB source models; we will therefore leave the detailed analysis on these topics for future studies.

Acknowledgments

Authors would like to thank Erik Floden, Vuk Mandic, Leo Tsukada and Gang Wang. R.D. is supported in part by the National Key R&D Program of China (No. 2021YFC2203100). C.T. is supported by the National Natural Science Foundation of China (Grants No. 12405048) and the Natural Science Foundation of Anhui Province (Grants No. 2308085QA34). The authors acknowledge the High-performance Computing Platform of Anhui University for providing computing resources.

A From the anisotropic GW fractional energy density to the GW intensity

In this appendix, we establish the relationship between the GW intensity multipoles $I_{\ell m}$ and the GW fractional energy multipoles $a_{\ell m}^{\rm GW}$. The metric perturbations $h_{ij}(t, \mathbf{x})$ can be expressed as a sum of contributions orginating from all directions in the sky via a plane-wave expansion:

$$h_{ij}(t, \mathbf{x}) = \int_{-\infty}^{\infty} df \int d^2\Omega_{\hat{\mathbf{n}}} \sum_{p=+,\times} h_p(f, \hat{\mathbf{n}}) \mathrm{e}_{ij}^{p}(\hat{\mathbf{n}}) e^{i2\pi f(t-\hat{\mathbf{n}}\cdot\mathbf{x})} \,, \tag{A.1}$$

where $p = \{+, \times\}$ labels the polarization states, $\hat{\mathbf{n}}$ represents the direction of propagation in the sky. The propagation direction $\hat{\mathbf{n}}$ along with two transverse directions $\hat{\boldsymbol{\theta}}$ and $\hat{\boldsymbol{\phi}}$ are

defined in terms of standard spherical coordinates:

$$\begin{aligned}
\hat{\mathbf{n}} &= \sin\theta\cos\phi\,\hat{\boldsymbol{x}} + \sin\theta\sin\phi\,\hat{\boldsymbol{y}} + \cos\theta\,\hat{\boldsymbol{z}}\,,\\
\hat{\boldsymbol{\theta}} &= \cos\theta\cos\phi\,\hat{\boldsymbol{x}} + \cos\theta\sin\phi\,\hat{\boldsymbol{y}} - \sin\theta\,\hat{\boldsymbol{z}}\,,\\
\hat{\boldsymbol{\phi}} &= -\sin\phi\,\hat{\boldsymbol{x}} + \cos\phi\,\hat{\boldsymbol{y}}\,.
\end{aligned} \tag{A.2}$$

With these coordinates, the GW polarization tensors are constructed as follows

$$e^{+}_{ij}(\hat{\mathbf{n}}) = \hat{\theta}_i\hat{\theta}_j - \hat{\phi}_i\hat{\phi}_j, \quad e^{\times}_{ij}(\hat{\mathbf{n}}) = \hat{\theta}_i\hat{\theta}_j + \hat{\phi}_i\hat{\phi}_j\,. \tag{A.3}$$

It is easy to check that they satisfy

$$\begin{aligned}
e^{+}_{ij}(\hat{\mathbf{n}})e^{+,ij}(\hat{\mathbf{n}}) &= e^{\times}_{ij}(\hat{\mathbf{n}})e^{\times,ij}(\hat{\mathbf{n}}) = 2\,,\\
e^{+}_{ij}(\hat{\mathbf{n}})e^{\times,ij}(\hat{\mathbf{n}}) &= e^{\times}_{ij}(\hat{\mathbf{n}})e^{+,ij}(\hat{\mathbf{n}}) = 0\,.
\end{aligned} \tag{A.4}$$

We thus obtain the orthogonal and normalization for the polarization tensors:

$$e^{p}_{ij}(\hat{\mathbf{n}})e^{p',ij}(\hat{\mathbf{n}}') = 2\delta_{pp'}\,. \tag{A.5}$$

Assuming that the GWB to be Gaussian, stationary, h_{ij} is characterized by its first and quadratic expectation values as

$$\left\langle h_p(f,\hat{\mathbf{n}})\right\rangle = 0\,, \tag{A.6}$$

$$\left\langle h_p(f,\hat{\mathbf{n}})h^{*}_{p'}\left(f',\hat{\mathbf{n}}'\right)\right\rangle \equiv \delta\left(f-f'\right)\frac{\delta^2\left(\hat{\mathbf{n}},\hat{\mathbf{n}}'\right)}{4\pi}\mathrm{W}_{pp'}(f,\hat{\mathbf{n}})\,, \tag{A.7}$$

where the matrix W is related to the gravitational Stokes parameters as

$$W(f,\hat{\mathbf{n}}) \equiv \begin{pmatrix} I(f,\hat{\mathbf{n}}) + Q(f,\hat{\mathbf{n}}) & U(f,\hat{\mathbf{n}}) - iV(f,\hat{\mathbf{n}}) \\ U(f,\hat{\mathbf{n}}) + iV(f,\hat{\mathbf{n}}) & I(f,\hat{\mathbf{n}}) - Q(f,\hat{\mathbf{n}}) \end{pmatrix}. \tag{A.8}$$

For unpolarized GW with $Q = U = V = 0$, Eq. A.7 is reduced to

$$\left\langle h_+(f,\hat{\mathbf{n}})h^{*}_{+}\left(f',\hat{\mathbf{n}}'\right)\right\rangle = \left\langle h_\times(f,\hat{\mathbf{n}})h^{*}_{\times}\left(f',\hat{\mathbf{n}}'\right)\right\rangle = \delta\left(f-f'\right)\frac{\delta^2\left(\hat{\mathbf{n}},\hat{\mathbf{n}}'\right)}{4\pi}I(f,\hat{\mathbf{n}})\,. \tag{A.9}$$

Inserting Eq. A.1 into expression of GW energy density $\rho_{\rm GW}$ and using Eq. A.9, we have

$$\begin{aligned}
\rho_{\rm GW} &= \frac{1}{32\pi G}\left\langle \dot{h}^{ij}\dot{h}_{ij}\right\rangle\\
&= \frac{1}{32\pi G}\int df\int df'\int d^2\Omega_{\hat{\mathbf{n}}}\int d^2\Omega_{\hat{\mathbf{n}}'}\sum_{p,p'}e^{p}_{ij}(\hat{\mathbf{n}})e^{p',ij}(\hat{\mathbf{n}}')(i2\pi f)(-i2\pi f')\\
&\quad\times\left\langle h_p(f,\hat{\mathbf{n}})h^{*}_{p'}\left(f',\hat{\mathbf{n}}'\right)\right\rangle e^{i2\pi(f-f')t}e^{i2\pi(f\hat{\mathbf{n}}-f'\hat{\mathbf{n}}')\cdot\mathbf{x}}\\
&= \frac{1}{8G}\int f^3 d\ln f\int d^2\Omega_{\hat{\mathbf{n}}}\,I(f,\hat{\mathbf{n}})\,.
\end{aligned} \tag{A.10}$$

Substituting above result into the definition of GWB spectrum $\Omega_{\rm GW}(f)$ and performing a spherical-harmonic decomposition of the intensity $I(f,\hat{\mathbf{n}})$, we arrive

$$\begin{aligned}\Omega_{\rm GW}(f) &\equiv \frac{1}{\rho_{\rm c}}\frac{d\rho_{\rm GW}}{d\ln f}\\ &= \frac{\pi}{3H_0^2}f^3\int d^2\Omega_{\hat{\mathbf{n}}}\sqrt{4\pi}\sum_{\ell=0}^{\ell_{\rm max}}\sum_{m=-\ell}^{\ell} I_{\ell m}(f)Y_{\ell m}(\hat{\mathbf{n}})\\ &= \frac{4\pi^2}{3H_0^2}f^3 I_{00}(f) + \sqrt{4\pi}\frac{\pi}{3H_0^2}f^3\int d^2\Omega_{\hat{\mathbf{n}}}\sum_{\ell=1}^{\ell_{\rm max}}\sum_{m=-\ell}^{\ell} I_{\ell m}(f)Y_{\ell m}(\hat{\mathbf{n}})\,, \end{aligned} \tag{A.11}$$

where we have introduced an additional $\sqrt{4\pi}$ factor to cancel Y_{00}, thereby ensuring the correspondence between the intensity monopole I_{00} and the monopole of GW energy fraction $\overline{\Omega}_{\rm GW}$. On the other hand, we also separate the GW spectrum into the background part (monopole) and the linear fluctuation $\delta_{\rm GW}$, then expanding the perturbation function with spherical harmonic basis:

$$\begin{aligned}\Omega_{\rm GW}(f) &= \frac{1}{4\pi}\int d^2\Omega_{\hat{\mathbf{n}}}\,\overline{\Omega}_{\rm GW}(f)\,[1+\delta_{\rm GW}(f,\hat{\mathbf{n}})]\\ &= \overline{\Omega}_{\rm GW}(f) + \frac{\overline{\Omega}_{\rm GW}(f)}{4\pi}\left(4-\frac{\partial\ln\overline{\Omega}_{\rm GW}(f)}{\partial\ln f}\right)\int d^2\Omega_{\hat{\mathbf{n}}}\sum_{\ell=1}^{\ell_{\rm max}}\sum_{m=-\ell}^{\ell} a_{\ell m}^{\rm GW}(f)Y_{\ell m}(\hat{\mathbf{n}})\,. \end{aligned} \tag{A.12}$$

Equating first terms in Eqs. A.11 and Eq. A.12 give the relationship between the intensity monopole $\overline{I}_{00}$ and the GW monopole $\overline{\Omega}_{\rm GW}$

$$\overline{I}_{00}(f) \equiv \frac{3H_0^2}{4\pi^2}\frac{\overline{\Omega}_{\rm GW}(f)}{f^3}\,, \tag{A.13}$$

while the second terms in Eqs. A.11 and Eq. A.12 show the relationship between the GW intensity multipoles $I_{\ell m}$ and the GW energy fraction multipoles $a_{\ell m}^{\rm GW}$:

$$\begin{aligned} I_{\ell m}(f) &= \frac{1}{\sqrt{4\pi}}\frac{3H_0^2}{4\pi^2}\frac{\overline{\Omega}_{\rm GW}(f)}{f^3}\left(4-\frac{\partial\ln\overline{\Omega}_{\rm GW}(f)}{\partial\ln f}\right)a_{\ell m}^{\rm GW}(f)\\ &= K_f a_{\ell m}^{\rm GW}(f)\,, \end{aligned} \tag{A.14}$$

where we have defined

$$K_f \equiv \frac{1}{\sqrt{4\pi}}\frac{3H_0^2}{4\pi^2}\frac{\overline{\Omega}_{\rm GW}(f)}{f^3}\left(4-\frac{\partial\ln\overline{\Omega}_{\rm GW}(f)}{\partial\ln f}\right). \tag{A.15}$$

From the auto-correlation function $\left\langle a_{\ell m}^{\rm GW} a_{\ell' m'}^{\rm GW*}\right\rangle = \delta_{\ell\ell'}\delta_{mm'}C_\ell^{\rm GW}$, we further obtain correspondence between the angular power spectrum of the GW intensity and energy fraction:

$$C_\ell^I(f) = K_f^2\, C_\ell^{\rm GW}(f)\,. \tag{A.16}$$

B Conditional probability distribution considering cross-correlations

A multidimensional complex Gaussian distribution for d-dimensional random variable $\boldsymbol{x}$ is given by

$$\mathcal{N}(\boldsymbol{\mu}, \boldsymbol{\Sigma}) = \frac{1}{\pi^d |\boldsymbol{\Sigma}|} \exp\left[-(\boldsymbol{x}-\boldsymbol{\mu})^T \boldsymbol{\Sigma}^{-1} (\boldsymbol{x}-\boldsymbol{\mu})\right] . \tag{B.1}$$

Suppose that the vector $\boldsymbol{x} = [\boldsymbol{x}_1^T, \boldsymbol{x}_2^T]^T$ obeys joint gaussian distribution

$$p(\boldsymbol{x}) \sim \mathcal{N}\left(\begin{bmatrix}\boldsymbol{\mu}_1 \\ \boldsymbol{\mu}_2\end{bmatrix}, \begin{bmatrix}\boldsymbol{\Sigma}_{11} & \boldsymbol{\Sigma}_{12} \\ \boldsymbol{\Sigma}_{12}^T & \boldsymbol{\Sigma}_{22}\end{bmatrix}\right) , \tag{B.2}$$

where $\boldsymbol{\Sigma}_{12}$ is the non-symmetric cross-covariance matrix between $\boldsymbol{x}_1$ and $\boldsymbol{x}_2$. Then the marginal distributions are

$$p(\boldsymbol{x}_1) = \int p(\boldsymbol{x}) d\boldsymbol{x}_2 \sim \mathcal{N}\left(\boldsymbol{\mu}_1, \boldsymbol{\Sigma}_{11}\right), \quad p(\boldsymbol{x}_2) = \int p(\boldsymbol{x}) d\boldsymbol{x}_1 \sim \mathcal{N}\left(\boldsymbol{\mu}_2, \boldsymbol{\Sigma}_{22}\right) , \tag{B.3}$$

and according to the definition, the conditional probability distributions are

$$\begin{aligned} p(\boldsymbol{x}_1|\boldsymbol{x}_2) &\sim \mathcal{N}\left(\boldsymbol{\mu}_1 + \boldsymbol{\Sigma}_{12}\boldsymbol{\Sigma}_{22}^{-1}(\boldsymbol{x}_2 - \boldsymbol{\mu}_2), \boldsymbol{\Sigma}_{11} - \boldsymbol{\Sigma}_{12}\boldsymbol{\Sigma}_{22}^{-1}\boldsymbol{\Sigma}_{12}^T\right) , \\ p(\boldsymbol{x}_2|\boldsymbol{x}_1) &\sim \mathcal{N}\left(\boldsymbol{\mu}_2 + \boldsymbol{\Sigma}_{12}^T\boldsymbol{\Sigma}_{11}^{-1}(\boldsymbol{x}_1 - \boldsymbol{\mu}_1), \boldsymbol{\Sigma}_{22} - \boldsymbol{\Sigma}_{12}^T\boldsymbol{\Sigma}_{11}^{-1}\boldsymbol{\Sigma}_{12}\right) . \end{aligned} \tag{B.4}$$

We now apply the results above to construct the likelihood function, incorporating the cross-correlations between the GWB and any known cosmological tracers. Assuming that the maps of GWB anisotropy and a set of cosmological tracers $\boldsymbol{Y}$, characterized by spherical harmonic coefficients $a_{\ell m}^{\rm GW}$ and $a_{\ell m}^{\boldsymbol{Y}}$ respectively, are multivariate Gaussian random variables with zero mean and covariance $C_\ell^{{\rm GW}\times\boldsymbol{Y}}$. Following eq. (B.2), their probability distribution is given by

$$p\left(a_{\{\ell m\}}^{\rm GW}, a_{\{\ell m\}}^{\boldsymbol{Y}}\right) = \prod_{\ell=1}^{\ell_{\rm max}} \prod_{m=-\ell}^{\ell} \frac{\exp\left\{-\begin{pmatrix} a_{\ell m}^{\rm GW} \\ a_{\ell m}^{\boldsymbol{Y}}\end{pmatrix}^T \begin{pmatrix} C_\ell^{\rm GW} & C_\ell^{{\rm GW}\times\boldsymbol{Y}} \\ C_\ell^{{\rm GW}\times\boldsymbol{Y}} & C_\ell^{\boldsymbol{Y}}\end{pmatrix}^{-1} \begin{pmatrix} a_{\ell m}^{\rm GW} \\ a_{\ell m}^{\boldsymbol{Y}}\end{pmatrix}\right\}}{\pi\left(C_\ell^{\rm GW} C_\ell^{\boldsymbol{Y}} - \left(C_\ell^{{\rm GW}\times\boldsymbol{Y}}\right)^2\right)} . \tag{B.5}$$

According to eq. (B.4), the conditional distribution of $a_{\ell m}^{\rm GW}$ for given $a_{\ell m}^{\boldsymbol{Y}}$ obeys

$$p\left(a_{\{\ell m\}}^{\rm GW}\middle| a_{\{\ell m\}}^{\boldsymbol{Y}}, \mu_{\{\ell m\}}^{{\rm GW}|\boldsymbol{Y}}, C_{\{\ell\}}^{{\rm GW}|\boldsymbol{Y}}\right) = \prod_{\ell=1}^{\ell_{\rm max}} \prod_{m=-\ell}^{\ell} \frac{\exp\left\{-\left(a_{\ell m}^{\rm GW} - \mu_{\ell m}^{{\rm GW}|\boldsymbol{Y}}\right)\left(C_\ell^{{\rm GW}|\boldsymbol{Y}}\right)^{-1}\left(a_{\ell m}^{\rm GW} - \mu_{\ell m}^{{\rm GW}|\boldsymbol{Y}}\right)\right\}}{\pi C_\ell^{{\rm GW}|\boldsymbol{Y}}} , \tag{B.6}$$

where the mean and the covariance are given by

$$\mu_{\ell m}^{{\rm GW}|\boldsymbol{Y}} = \frac{C_\ell^{{\rm GW}\times\boldsymbol{Y}}}{C_\ell^{\boldsymbol{Y}}} a_{\ell m}^{\boldsymbol{Y}} , \tag{B.7}$$

$$C_\ell^{{\rm GW}|\boldsymbol{Y}} = C_\ell^{\rm GW} - \frac{\left(C_\ell^{{\rm GW}\times\boldsymbol{Y}}\right)^2}{C_\ell^{\boldsymbol{Y}}} = C_\ell^{\rm GW}\left[1 - \left(\frac{C_\ell^{{\rm GW}\times\boldsymbol{Y}}}{\sqrt{C_\ell^{\rm GW} C_\ell^{\boldsymbol{Y}}}}\right)^2\right] . \tag{B.8}$$

From now on, for simplicity, we will focus on a single tracer, Y, instead of a set of tracers, $\boldsymbol{Y}$, although the generalization to multiple tracers is straightforward. Using eq. (2.3), we obtain the likelihood for the GWB intensity

$$\begin{aligned}\mathcal{L}\left(I_{\{\ell m\},f} \mid \mathrm{GW}\times\mathrm{Y}\right) &\equiv p\Big(I_{\{\ell m\},f}\Big|a^{\mathrm{Y}}_{\{\ell m\}},\mu^{\mathrm{GW|Y}}_{\{\ell m\}},C^{\mathrm{GW|Y}}_{\{\ell\}}\Big)\\ &=\prod_{\ell=1}^{\ell_{\max}}\prod_{m=-\ell}^{\ell}\frac{\exp\left\{-\left(I_{\ell m}-K_f\mu^{\mathrm{GW|Y}}_{\ell m}\right)\left(K_f^2C^{\mathrm{GW|Y}}_{\ell}\right)^{-1}\left(I_{\ell m}-K_f\mu^{\mathrm{GW|Y}}_{\ell m}\right)\right\}}{\pi C^{\mathrm{GW|Y}}_{\ell}}\,.\end{aligned}\tag{B.9}$$

C Likelihood function after marginalization

Utilizing the complex Gaussian integration formula

$$\int d^{2d}\boldsymbol{z}\exp\left(-\boldsymbol{z}^\dagger\boldsymbol{M}\boldsymbol{z}+\boldsymbol{K}^\dagger\boldsymbol{z}+\boldsymbol{z}^\dagger\boldsymbol{K}+\boldsymbol{Q}\right)=\frac{\pi^d}{|\boldsymbol{M}|}\exp\left(\boldsymbol{K}^\dagger\boldsymbol{M}^{-1}\boldsymbol{K}+\boldsymbol{Q}\right),\tag{C.1}$$

the likelihood eq. (3.8) reads

$$\mathcal{L}\Big(D_{\{t,f\}}\Big|\mathrm{GW}\times\mathrm{Y}\Big)=\prod_{t,f}\frac{1}{|\pi C_D||C_I||M|}\exp\left(K^\dagger_\mu M^{-1}_{\mu\nu}K_\nu+Q\right),\tag{C.2}$$

$$M^{-1}_{\mu\nu}=\left((C_I)^{-1}_{\mu\nu}+\Gamma^*_{\mu a}(C_D)^{-1}_{ab}\Gamma_{b\nu}\right)^{-1},\tag{C.3}$$

$$K_\mu=\Gamma^*_{\mu a}(C_D)^{-1}_{ab}\Big(D_b-\Gamma_{b0}\overline{X}_0-N_b\Big)+(C_I)^{-1}_{\mu\nu}\overline{X}_\nu\,,\tag{C.4}$$

$$Q=-\left(D_a-\overline{X}_0\Gamma_{0a}-N_a\right)^*(C_D)^{-1}_{ab}\left(D_b-\Gamma_{b0}\overline{X}_0-N_b\right)-\overline{X}^\dagger_\mu(C_I)^{-1}_{\mu\nu}\overline{X}_\nu\,.\tag{C.5}$$

We will show that eq. (C.2) can be reformulated into a more concise expression, providing a clearer representation of the underlying physics. To see this, we employ Sherman-Morrison-Woodbury matrix inversion lemma, written as

$$\left(\boldsymbol{A}+\boldsymbol{X}\boldsymbol{B}\boldsymbol{X}^\dagger\right)^{-1}=\boldsymbol{A}^{-1}-\boldsymbol{A}^{-1}\boldsymbol{X}\left(\boldsymbol{B}^{-1}+\boldsymbol{X}^\dagger\boldsymbol{A}^{-1}\boldsymbol{X}\right)^{-1}\boldsymbol{X}^\dagger\boldsymbol{A}^{-1},\tag{C.6}$$

$$\left|\boldsymbol{A}+\boldsymbol{X}\boldsymbol{B}\boldsymbol{X}^\dagger\right|=\left|\boldsymbol{B}\right|\left|\boldsymbol{A}\right|\left|\boldsymbol{B}^{-1}+\boldsymbol{X}^\dagger\boldsymbol{A}^{-1}\boldsymbol{X}\right|,\tag{C.7}$$

where $\boldsymbol{A}$ and $\boldsymbol{B}$ are square and invertible matrices, though not necessarily have the same dimension. From which, adopting the matrix form for simplicity, we obtain following relations:

$$\begin{aligned}\left(C_D+\Gamma C_I\Gamma^\dagger\right)^{-1}&=C_D^{-1}-C_D^{-1}\Gamma\left(C_I^{-1}+\Gamma^\dagger C_D^{-1}\Gamma\right)^{-1}\Gamma^\dagger C_D^{-1}\\&\simeq C_D^{-1}-C_D^{-1}\Gamma C_I\Gamma^\dagger C_D^{-1}\,,\end{aligned}\tag{C.8}$$

$$\begin{aligned}\left(C_I^{-1}+\Gamma^\dagger C_D^{-1}\Gamma\right)^{-1}&=C_I-C_I\Gamma^+\left(C_D+\Gamma C_I\Gamma^\dagger\right)^{-1}\Gamma C_I\\&\simeq C_I-C_I\Gamma^\dagger C_D^{-1}\Gamma C_I\,,\end{aligned}\tag{C.9}$$

$$\begin{aligned}|C_D||C_I||M|&=|C_D||C_I||C_I^{-1}+\Gamma^\dagger C_D^{-1}\Gamma|\\&=\left|C_D+\Gamma C_I\Gamma^\dagger\right|.\end{aligned}\tag{C.10}$$

Following these relations, the exponential term in eq. (C.2) can be rearranged to get

$$
\begin{aligned}
&K_\mu^\dagger M_{\mu\nu}^{-1} K_\nu + Q \\
=&\left[\left(D_a - \Gamma_0 \overline{X}_0 - N_a\right)^\dagger C_D^{-1}\Gamma + \overline{X}^\dagger C_I^{-1}\right] \left(C_I^{-1} + \Gamma^\dagger C_D^{-1}\Gamma\right)^{-1} \left[\Gamma^\dagger C_D^{-1}\left(D_b - \Gamma_0\overline{X}_0 - N_b\right) + C_I^{-1}\overline{X}\right] \\
&- \left(D_a - \Gamma_0 \overline{X}_0 - N_a\right)^\dagger C_D^{-1}\left(D_b - \Gamma_0\overline{X}_0 - N_b\right) - \overline{X}^\dagger C_I^{-1}\overline{X} \\
=&- \left(D_a - \Gamma_0 \overline{X}_0 - N_a\right)^\dagger \left[C_D^{-1} - C_D^{-1}\Gamma\left(C_I^{-1} + \Gamma^\dagger C_D^{-1}\Gamma\right)^{-1}\Gamma^\dagger C_D^{-1}\right]\left(D_b - \Gamma_0\overline{X}_0 - N_b\right) \\
&+ \left(D_a - \Gamma_0 \overline{X}_0 - N_a\right)^\dagger C_D^{-1}\Gamma\left(C_I^{-1} + \Gamma^\dagger C_D^{-1}\Gamma\right)^{-1} C_I^{-1}\overline{X} \\
&+ \overline{X}^\dagger C_I^{-1}\left(C_I^{-1} + \Gamma^\dagger C_D^{-1}\Gamma\right)^{-1}\Gamma^\dagger C_D^{-1}\left(D_b - \Gamma_0\overline{X}_0 - N_b\right) \\
&+ \overline{X}^\dagger C_I^{-1}\left(C_I^{-1} + \Gamma^\dagger C_D^{-1}\Gamma\right)^{-1} C_I^{-1}\overline{X} - \overline{X}^\dagger C_I^{-1}\overline{X} \\
\simeq&- \left(D_a - \Gamma_0 \overline{X}_0 - N_a\right)^\dagger \left(C_D + \Gamma C_I \Gamma^\dagger\right)^{-1}\left(D_b - \Gamma_0\overline{X}_0 - N_b\right) \\
&+ \left(D_a - \Gamma_0 \overline{X}_0 - N_a\right)^\dagger \left(C_D + \Gamma C_I \Gamma^\dagger\right)^{-1}\Gamma\overline{X} \\
&+ \overline{X}^\dagger\Gamma^\dagger\left(C_D + \Gamma C_I \Gamma^\dagger\right)^{-1}\left(D_b - \Gamma_0\overline{X}_0 - N_b\right) \\
&- \overline{X}^\dagger\Gamma^\dagger\left(C_D + \Gamma C_I \Gamma^\dagger\right)^{-1}\Gamma\overline{X} \\
=&- \left(D_a - \Gamma_0 \overline{X}_0 - N_a - \Gamma\overline{X}\right)^\dagger \left(C_D + \Gamma C_I \Gamma^\dagger\right)^{-1}\left(D_b - \Gamma_0\overline{X}_0 - N_b - \Gamma\overline{X}\right) .
\end{aligned}
\tag{C.11}
$$

Taking into account the determinants, eq. (C.2) then becomes

$$
\begin{aligned}
&\mathcal{L}\Big(D_{\{t,f\}}\Big|\mathrm{GW}\times\mathrm{Y}\Big) \\
&= \prod_{t,f}\frac{1}{\left|\pi(C_D + \Gamma C_I\Gamma^\dagger)\right|}\exp\Big\{ - \left(D_a - \Gamma_0\overline{X}_0 - N_a - \Gamma\overline{X}\right)^\dagger\left(C_D + \Gamma C_I\Gamma^\dagger\right)^{-1}\left(D_b - \Gamma_0\overline{X}_0 - N_b - \Gamma\overline{X}\right)\Big\} .
\end{aligned}
\tag{C.12}
$$

Finally, to combine two terms associated with $\overline{X}$, we define $\overline{Z}_\mu \equiv \overline{X}_\mu$ for $\mu \geq 1$ and $\overline{Z}_0 \equiv \overline{X}_0$ for $\mu = 0$, and redefine

$$
(C_I)_{\mu\nu} \equiv K_f^2 \mathrm{diag}\Big(\underbrace{0, C_1^{\mathrm{GW|Y}}, C_1^{\mathrm{GW|Y}}, C_1^{\mathrm{GW|Y}}, \cdots, \overbrace{C_{\ell_{\max}}^{\mathrm{GW|Y}}, \cdots, C_{\ell_{\max}}^{\mathrm{GW|Y}}}^{(2\ell_{\max}+1)\text{ terms}}}_{(\ell_{\max}+1)^2\text{ terms}}\Big) ,
\tag{C.13}
$$

to match the matrix dimensions, arriving the likelihood function in eq. (3.9)

$$
\mathcal{L}\left(D_{\{t,f\}} \mid \mathrm{GW}\times\mathrm{Y}\right) \propto \prod_{t,f}\left|\pi C_{ab}\right|^{-1}\exp\left(-J_a^\dagger C_{ab}^{-1} J_b\right) ,
\tag{C.14}
$$

$$
C_{ab} = (C_D)_{ab} + \Gamma_{a\mu}(C_I)_{\mu\nu}\Gamma^*_{\nu b} ,
\tag{C.15}
$$

$$
J_a = D_a - \Gamma_{a\mu}\overline{Z}_\mu - N_a .
\tag{C.16}
$$

References

[1] NANOGrav collaboration, *The NANOGrav 15 yr Data Set: Evidence for a Gravitational-wave Background*, *Astrophys. J. Lett.* **951** (2023) L8 [2306.16213].

[2] H. Xu et al., *Searching for the Nano-Hertz Stochastic Gravitational Wave Background with the Chinese Pulsar Timing Array Data Release I*, *Res. Astron. Astrophys.* **23** (2023) 075024 [2306.16216].

[3] EPTA collaboration, *The second data release from the European Pulsar Timing Array III. Search for gravitational wave signals*, 2306.16214.

[4] D.J. Reardon et al., *Search for an Isotropic Gravitational-wave Background with the Parkes Pulsar Timing Array*, *Astrophys. J. Lett.* **951** (2023) L6 [2306.16215].

[5] M.T. Miles et al., *The MeerKAT Pulsar Timing Array: The first search for gravitational waves with the MeerKAT radio telescope*, 2412.01153.

[6] V. Ferrari, S. Matarrese and R. Schneider, *Stochastic background of gravitational waves generated by a cosmological population of young, rapidly rotating neutron stars*, *Mon. Not. Roy. Astron. Soc.* **303** (1999) 258 [astro-ph/9806357].

[7] V. Ferrari, S. Matarrese and R. Schneider, *Gravitational wave background from a cosmological population of core collapse supernovae*, *Mon. Not. Roy. Astron. Soc.* **303** (1999) 247 [astro-ph/9804259].

[8] R. Schneider, V. Ferrari, S. Matarrese and S.F. Portegies Zwart, *Gravitational waves from cosmological compact binaries*, *Mon. Not. Roy. Astron. Soc.* **324** (2001) 797 [astro-ph/0002055].

[9] A.J. Farmer and E.S. Phinney, *The gravitational wave background from cosmological compact binaries*, *Mon. Not. Roy. Astron. Soc.* **346** (2003) 1197 [astro-ph/0304393].

[10] T. Regimbau, *The astrophysical gravitational wave stochastic background*, *Res. Astron. Astrophys.* **11** (2011) 369 [1101.2762].

[11] X.-J. Zhu, E. Howell, T. Regimbau, D. Blair and Z.-H. Zhu, *Stochastic Gravitational Wave Background from Coalescing Binary Black Holes*, *Astrophys. J.* **739** (2011) 86 [1104.3565].

[12] T. Vachaspati and A. Vilenkin, *Gravitational Radiation from Cosmic Strings*, *Phys. Rev. D* **31** (1985) 3052.

[13] A. Kosowsky, M.S. Turner and R. Watkins, *Gravitational waves from first order cosmological phase transitions*, *Phys. Rev. Lett.* **69** (1992) 2026.

[14] M.C. Guzzetti, N. Bartolo, M. Liguori and S. Matarrese, *Gravitational waves from inflation*, *Riv. Nuovo Cim.* **39** (2016) 399 [1605.01615].

[15] C. Caprini and D.G. Figueroa, *Cosmological Backgrounds of Gravitational Waves*, *Class. Quant. Grav.* **35** (2018) 163001 [1801.04268].

[16] N. Aggarwal et al., *Challenges and opportunities of gravitational-wave searches at MHz to GHz frequencies*, *Living Rev. Rel.* **24** (2021) 4 [2011.12414].

[17] V. Alba and J. Maldacena, *Primordial gravity wave background anisotropies*, *JHEP* **03** (2016) 115 [1512.01531].

[18] J. Liu, R.-G. Cai and Z.-K. Guo, *Large Anisotropies of the Stochastic Gravitational Wave Background from Cosmic Domain Walls*, *Phys. Rev. Lett.* **126** (2021) 141303 [2010.03225].

[19] C.R. Contaldi, *Anisotropies of Gravitational Wave Backgrounds: A Line Of Sight Approach*, *Phys. Lett. B* **771** (2017) 9 [1609.08168].

[20] M. Geller, A. Hook, R. Sundrum and Y. Tsai, *Primordial Anisotropies in the Gravitational Wave Background from Cosmological Phase Transitions*, *Phys. Rev. Lett.* **121** (2018) 201303 [1803.10780].

[21] N. Bartolo, D. Bertacca, S. Matarrese, M. Peloso, A. Ricciardone, A. Riotto et al., *Anisotropies and non-Gaussianity of the Cosmological Gravitational Wave Background*, *Phys. Rev. D* **100** (2019) 121501 [1908.00527].

[22] N. Bartolo, D. Bertacca, S. Matarrese, M. Peloso, A. Ricciardone, A. Riotto et al., *Characterizing the cosmological gravitational wave background: Anisotropies and non-Gaussianity*, *Phys. Rev. D* **102** (2020) 023527 [1912.09433].

[23] L. Valbusa Dall'Armi, A. Ricciardone, N. Bartolo, D. Bertacca and S. Matarrese, *Imprint of relativistic particles on the anisotropies of the stochastic gravitational-wave background*, *Phys. Rev. D* **103** (2021) 023522 [2007.01215].

[24] Y. Li, F.P. Huang, X. Wang and X. Zhang, *Anisotropy of phase transition gravitational wave and its implication for primordial seeds of the Universe*, *Phys. Rev. D* **105** (2022) 083527 [2112.01409].

[25] F. Schulze, L. Valbusa Dall'Armi, J. Lesgourgues, A. Ricciardone, N. Bartolo, D. Bertacca et al., *GW_CLASS: Cosmological Gravitational Wave Background in the Cosmic Linear Anisotropy Solving System*, 2305.01602.

[26] Y. Cui, S. Kumar, R. Sundrum and Y. Tsai, *Unraveling Cosmological Anisotropies within Stochastic Gravitational Wave Backgrounds*, 2307.10360.

[27] S. Wang, Z.-C. Zhao, J.-P. Li and Q.-H. Zhu, *Implications of Pulsar Timing Array Data for Scalar-Induced Gravitational Waves and Primordial Black Holes: Primordial Non-Gaussianity $f_{\rm NL}$ Considered*, 2307.00572.

[28] J.-P. Li, S. Wang, Z.-C. Zhao and K. Kohri, *Primordial Non-Gaussianity $f_{\rm NL}$ and Anisotropies in Scalar-Induced Gravitational Waves*, 2305.19950.

[29] L. Valbusa Dall'Armi, A. Nishizawa, A. Ricciardone and S. Matarrese, *Circular Polarization of the Astrophysical Gravitational Wave Background*, *Phys. Rev. Lett.* **131** (2023) 041401 [2301.08205].

[30] L. Bethke, D.G. Figueroa and A. Rajantie, *Anisotropies in the Gravitational Wave Background from Preheating*, *Phys. Rev. Lett.* **111** (2013) 011301 [1304.2657].

[31] G. Cusin, C. Pitrou and J.-P. Uzan, *Anisotropy of the astrophysical gravitational wave background: Analytic expression of the angular power spectrum and correlation with cosmological observations*, *Phys. Rev. D* **96** (2017) 103019 [1704.06184].

[32] G. Cusin, I. Dvorkin, C. Pitrou and J.-P. Uzan, *First predictions of the angular power spectrum of the astrophysical gravitational wave background*, *Phys. Rev. Lett.* **120** (2018) 231101 [1803.03236].

[33] A.C. Jenkins, R. O'Shaughnessy, M. Sakellariadou and D. Wysocki, *Anisotropies in the astrophysical gravitational-wave background: The impact of black hole distributions*, *Phys. Rev. Lett.* **122** (2019) 111101 [1810.13435].

[34] G. Cusin, I. Dvorkin, C. Pitrou and J.-P. Uzan, *Properties of the stochastic astrophysical gravitational wave background: astrophysical sources dependencies*, *Phys. Rev. D* **100** (2019) 063004 [1904.07797].

[35] D. Bertacca, A. Ricciardone, N. Bellomo, A.C. Jenkins, S. Matarrese, A. Raccanelli et al., *Projection effects on the observed angular spectrum of the astrophysical stochastic gravitational wave background*, *Phys. Rev. D* **101** (2020) 103513 [1909.11627].

[36] N. Bellomo, D. Bertacca, A.C. Jenkins, S. Matarrese, A. Raccanelli, T. Regimbau et al., *CLASS_GWB: robust modeling of the astrophysical gravitational wave background anisotropies*, *JCAP* **06** (2022) 030 [2110.15059].

[37] G. Sato-Polito and M. Kamionkowski, *Exploring the spectrum of stochastic gravitational-wave anisotropies with pulsar timing arrays*, 2305.05690.

[38] N. Pol, S.R. Taylor and J.D. Romano, *Forecasting Pulsar Timing Array Sensitivity to Anisotropy in the Stochastic Gravitational Wave Background*, *Astrophys. J.* **940** (2022) 173 [2206.09936].

[39] A. Malhotra, E. Dimastrogiovanni, G. Domènech, M. Fasiello and G. Tasinato, *New universal property of cosmological gravitational wave anisotropies*, *Phys. Rev. D* **107** (2023) 103502 [2212.10316].

[40] Y.-H. Yu and S. Wang, *Anisotropies in scalar-induced gravitational-wave background from inflaton-curvaton mixed scenario with sound speed resonance*, *Phys. Rev. D* **109** (2024) 083501 [2310.14606].

[41] R.-G. Cai, S.-J. Wang, Z.-Y. Yuwen and X.-X. Zeng, *Anisotropies of cosmological gravitational wave backgrounds in non-flat spacetime*, 2410.17721.

[42] D. Alonso, G. Cusin, P.G. Ferreira and C. Pitrou, *Detecting the anisotropic astrophysical gravitational wave background in the presence of shot noise through cross-correlations*, *Phys. Rev. D* **102** (2020) 023002 [2002.02888].

[43] D. Alonso, C.R. Contaldi, G. Cusin, P.G. Ferreira and A.I. Renzini, *Noise angular power spectrum of gravitational wave background experiments*, *Phys. Rev. D* **101** (2020) 124048 [2005.03001].

[44] A. Ricciardone, L.V. Dall'Armi, N. Bartolo, D. Bertacca, M. Liguori and S. Matarrese, *Cross-Correlating Astrophysical and Cosmological Gravitational Wave Backgrounds with the Cosmic Microwave Background*, *Phys. Rev. Lett.* **127** (2021) 271301 [2106.02591].

[45] G. Capurri, A. Lapi and C. Baccigalupi, *Detectability of the Cross-Correlation between CMB Lensing and Stochastic GW Background from Compact Object Mergers*, *Universe* **8** (2022) 160 [2111.04757].

[46] A.C. Jenkins, M. Sakellariadou, T. Regimbau and E. Slezak, *Anisotropies in the astrophysical gravitational-wave background: Predictions for the detection of compact binaries by LIGO and Virgo*, *Phys. Rev. D* **98** (2018) 063501 [1806.01718].

[47] Z.-C. Zhao and S. Wang, *Measuring the anisotropies in astrophysical and cosmological gravitational-wave backgrounds with Taiji and LISA networks*, *Sci. China Phys. Mech. Astron.* **67** (2024) 120411 [2407.09380].

[48] G. Capurri, A. Lapi, L. Boco and C. Baccigalupi, *Searching for Anisotropic Stochastic Gravitational-wave Backgrounds with Constellations of Space-based Interferometers*, *Astrophys. J.* **943** (2023) 72 [2212.06162].

[49] A.I. Renzini and C.R. Contaldi, *Mapping Incoherent Gravitational Wave Backgrounds*, *Mon. Not. Roy. Astron. Soc.* **481** (2018) 4650 [1806.11360].

[50] A. Renzini and C. Contaldi, *Improved limits on a stochastic gravitational-wave background and its anisotropies from Advanced LIGO O1 and O2 runs*, *Phys. Rev. D* **100** (2019) 063527 [1907.10329].

[51] S. Banagiri, A. Criswell, T. Kuan, V. Mandic, J.D. Romano and S.R. Taylor, *Mapping the gravitational-wave sky with lisa: a bayesian spherical harmonic approach*, *Monthly Notices of the Royal Astronomical Society* **507** (2021) 5451–5462.

[52] LISA Cosmology Working Group collaboration, *Probing anisotropies of the Stochastic Gravitational Wave Background with LISA*, *JCAP* **11** (2022) 009 [2201.08782].

[53] A.K.-W. Chung and N. Yunes, *Untargeted Bayesian search of anisotropic gravitational-wave backgrounds through the analytical marginalization of the posterior*, *Phys. Rev. D* **108** (2023) 043032 [2305.06502].

[54] L. Tsukada, S. Jaraba, D. Agarwal and E. Floden, *Bayesian parameter estimation for targeted anisotropic gravitational-wave background*, *Phys. Rev. D* **107** (2023) 023024 [2208.14421].

[55] J. Gair, J.D. Romano, S. Taylor and C.M.F. Mingarelli, *Mapping gravitational-wave backgrounds using methods from CMB analysis: Application to pulsar timing arrays*, *Phys. Rev. D* **90** (2014) 082001 [1406.4664].

[56] Z.-Y. Li, Z.-C. Liang, E.-K. Li, J.-d. Zhang and Y.-M. Hu, *Mapping Anisotropies in the Stochastic Gravitational-Wave Background with TianQin*, 2409.11245.

[57] NANOGrav collaboration, *The NANOGrav 15-year Data Set: Search for Anisotropy in the Gravitational-Wave Background*, 2306.16221.

[58] P. Adshead, N. Afshordi, E. Dimastrogiovanni, M. Fasiello, E.A. Lim and G. Tasinato, *Multimessenger cosmology: Correlating cosmic microwave background and stochastic gravitational wave background measurements*, *Phys. Rev. D* **103** (2021) 023532 [2004.06619].

[59] R. Ding and C. Tian, *On the anisotropies of the cosmological gravitational-wave background from pulsar timing array observations*, *JCAP* **02** (2024) 016 [2309.01643].

[60] K.Z. Yang, J. Suresh, G. Cusin, S. Banagiri, N. Feist, V. Mandic et al., *Measurement of the cross-correlation angular power spectrum between the stochastic gravitational wave background and galaxy overdensity*, *Phys. Rev. D* **108** (2023) 043025 [2304.07621].

[61] LISA collaboration, *Laser Interferometer Space Antenna*, 1702.00786.

[62] LISA collaboration, *New horizons for fundamental physics with LISA*, *Living Rev. Rel.* **25** (2022) 4 [2205.01597].

[63] LISA collaboration, *LISA Definition Study Report*, 2402.07571.

[64] T.L. Smith, T.L. Smith, R.R. Caldwell and R. Caldwell, *LISA for Cosmologists: Calculating the Signal-to-Noise Ratio for Stochastic and Deterministic Sources*, *Phys. Rev. D* **100** (2019) 104055 [1908.00546].

[65] E. Thrane, S. Ballmer, J.D. Romano, S. Mitra, D. Talukder, S. Bose et al., *Probing the anisotropies of a stochastic gravitational-wave background using a network of ground-based laser interferometers*, *Phys. Rev. D* **80** (2009) 122002 [0910.0858].

[66] J.D. Romano and N.J. Cornish, *Detection methods for stochastic gravitational-wave backgrounds: a unified treatment*, *Living Rev. Rel.* **20** (2017) 2 [1608.06889].

[67] H. Kurki-Suonio, V. Muhonen and J. Väliviita, *Correlated primordial perturbations in light of cmb and large scale structure data*, *Phys. Rev. D* **71** (2005) 063005.

[68] C.M. Hirata, S. Ho, N. Padmanabhan, U.c.v. Seljak and N.A. Bahcall, *Correlation of cmb with large-scale structure. ii. weak lensing*, *Phys. Rev. D* **78** (2008) 043520.

[69] W. Hu and R. Scranton, *Measuring dark energy clustering with CMB-galaxy correlations*, *Phys. Rev. D* **70** (2004) 123002 [astro-ph/0408456].

[70] R. van Haasteren and Y. Levin, *Understanding and analysing time-correlated stochastic signals in pulsar timing*, *Mon. Not. Roy. Astron. Soc.* **428** (2013) 1147 [1202.5932].

[71] LISA Cosmology Working Group collaboration, *Gravitational waves from first-order phase transitions in LISA: reconstruction pipeline and physics interpretation*, *JCAP* **10** (2024) 020 [2403.03723].

[72] N. Bartolo et al., *Science with the space-based interferometer LISA. IV: Probing inflation with gravitational waves*, *JCAP* **12** (2016) 026 [1610.06481].

[73] K.M. Górski, E. Hivon, A.J. Banday, B.D. Wandelt, F.K. Hansen, M. Reinecke et al., *HEALPix - A Framework for high resolution discretization, and fast analysis of data distributed on the sphere*, *Astrophys. J.* **622** (2005) 759 [astro-ph/0409513].

[74] L.J. Rubbo, N.J. Cornish and O. Poujade, *Forward modeling of space borne gravitational wave detectors*, *Phys. Rev. D* **69** (2004) 082003 [gr-qc/0311069].

[75] R.C. Bernardo and K.-W. Ng, *Pulsar and cosmic variances of pulsar timing-array correlation measurements of the stochastic gravitational wave background*, *JCAP* **11** (2022) 046 [2209.14834].

[76] LIGO Scientific, Virgo collaboration, *Upper Limits on the Stochastic Gravitational-Wave Background from Advanced LIGO's First Observing Run*, *Phys. Rev. Lett.* **118** (2017) 121101 [1612.02029].

[77] TianQin collaboration, *TianQin: a space-borne gravitational wave detector*, *Class. Quant. Grav.* **33** (2016) 035010 [1512.02076].

[78] W.-R. Hu and Y.-L. Wu, *The Taiji Program in Space for gravitational wave physics and the nature of gravity*, *Natl. Sci. Rev.* **4** (2017) 685.

[79] W.-H. Ruan, Z.-K. Guo, R.-G. Cai and Y.-Z. Zhang, *Taiji program: Gravitational-wave sources*, *Int. J. Mod. Phys. A* **35** (2020) 2050075 [1807.09495].

[80] S. Kawamura et al., *The Japanese space gravitational wave antenna: DECIGO*, *Class. Quant. Grav.* **28** (2011) 094011.

[81] V. Corbin and N.J. Cornish, *Detecting the cosmic gravitational wave background with the big bang observer*, *Class. Quant. Grav.* **23** (2006) 2435 [gr-qc/0512039].

[82] M. Maggiore et al., *Science Case for the Einstein Telescope*, *JCAP* **03** (2020) 050 [1912.02622].

[83] A. Torres-Orjuela, S.-J. Huang, Z.-C. Liang, S. Liu, H.-T. Wang, C.-Q. Ye et al., *Detection of astrophysical gravitational wave sources by TianQin and LISA*, *Sci. China Phys. Mech. Astron.* **67** (2024) 259511 [2307.16628].

[84] A. Torres-Orjuela, *Joint gravitational wave detection by TianQin and LISA*, in *7th International Workshop on the TianQin Science Mission*, 7, 2024 [2407.11293].

[85] Z.-C. Liang, Z.-Y. Li, E.-K. Li, J.-d. Zhang and Y.-M. Hu, *Unveiling a multi-component stochastic gravitational-wave background with the TianQin + LISA network*, 2409.00778.